Production and study of high-beta plasma confined by a superconducting dipole magnet

D. T. Garnier,* A. Hansen, M. E. Mauel, and E. Ortiz
Department of Applied Physics and Applied Mathematics
Columbia University, New York, NY 10027

A. Boxer, J. Ellsworth, I. Karim, J. Kesner, S. Mahar, and A. Roach
Plasma Science and Fusion Center, MIT, Cambridge, MA 02139
(Dated: October 28, 2005)

The Levitated Dipole Experiment (LDX) [J. Kesner, *et al.* in *Fusion Energy 1998* **3**, 1165 (1999)] is a new research facility that is exploring the confinement and stability of plasma created within the dipole field produced by a strong superconducting magnet. Unlike other configurations in which stability depends on curvature and magnetic shear, magnetohydrodynamic stability of a dipole derives from plasma compressibility. Theoretically, the dipole magnetic geometry can stabilize a centrally-peaked plasma pressure that exceeds the local magnetic pressure ($\beta > 1$), and the absence of magnetic shear allows particle and energy confinement to decouple. In initial experiments, long-pulse, quasi-steadystate microwave discharges lasting more than 10 seconds have been produced that are consistent with equilibria having peak beta values of 20%. Detailed measurements have been made of discharge evolution, plasma dynamics and instability, and the roles of gas fueling, microwave power deposition profiles, and plasma boundary shape. In these initial experiments, the high-field superconducting floating coil was supported by three thin supports. The plasma is created by multi-frequency electron cyclotron resonance heating at 2.45 and 6.4 GHz, and a population of energetic electrons, with mean energies above 50 keV, dominates the plasma pressure. Creation of high-pressure, high-beta plasma is possible only when intense hot electron interchange instabilities are stabilized by sufficiently high background plasma density. A dramatic transition from a low-density, low-beta regime to a more quiescent, high-beta regime is observed when the plasma fueling rate and confinement time become sufficiently large.

PACS numbers: 52.55.-s, 52.50.SW, 52.35.-g

I. INTRODUCTION

The Levitated Dipole Experiment (LDX), shown in Fig. 1, is a new research facility that was designed to investigate the confinement and stability of plasma in a dipole magnetic field configuration.[1] The dipole confinement concept was motivated by spacecraft observations of planetary magnetospheres that show centrally-peaked plasma pressure profiles forming naturally when the solar wind drives plasma circulation and heating.[2] Unlike most other approaches to magnetic confinement in which stability requires average good curvature and magnetic shear, magnetohydrodynamic (MHD) stability in a dipole derives from plasma compressibility.[3–5] Plasma is stable to interchange and ballooning instabilities when the pressure gradient is sufficiently gentle even when the local plasma pressure exceeds the magnetic pressure or, equivalently, when $\beta \equiv 2\mu_0 p/B^2 > 1$.[6] The ability of the dipole configuration to confine a high-beta plasma without magnetic shear may decouple particle and energy confinement, avoid the accumulation of fusion reaction products, and enable the dipole fusion power concept to operate with a ^{3}He catalyzed D-D fuel cycle.[7]

In this article we report the first experiments using the LDX device and describe the production of high beta plasma confined by a dipole magnet using neutral gas fueling and electron cyclotron resonance heating (ECRH). The pressure results from a population of energetic trapped electrons that can be maintained for many seconds of microwave heating provided sufficient neutral gas is supplied to the plasma.

A number of previous experiments also used ECRH to produce high beta plasma.[8,9,11,12] Energetic trapped electrons were first generated in the ELMO experiments[8] where harmonic cyclotron absorption created a localized "ring" of weakly relativistic electrons ($E_h \sim 400$ keV) within a plasma containing a larger density of cooler electrons. Linked magnetic mirrors, in which high beta electron rings were created, formed the bumpy torus device (EBT).[9] In simple axisymmetric mirrors, internal magnetic probes were able to characterize the plasma equilibrium, and, during optimal conditions, multiple-frequency ECRH[11] produced anisotropic plasmas that reached high values of local beta, $\beta \approx 40\%$, and high ratios of the perpendicular and parallel pressures, $\beta_\perp/\beta_{||} \approx 4.3$. A similar study using a non-axisymmetric, minimum-B, magnetic mirror[12] also achieved $\beta \approx 35\%$ with weakly relativistic electrons having anisotropic pressure $\beta_\perp/\beta_{||} \gg 1$.

Early heating experiments, like those in EBT, were done in "long-thin" unstable mirrors in which stabilizing plasma compressibility effects were insignificant. The stability of the background plasma in EBT was believed to depend on a diamagnetic well created by the hot electron ring, and stability of the hot electron ring depended on having a critical background plasma density. This

symbiotic relationship resulted in a relatively restricted stable operating regime (in terms of neutral gas pressure). Additionally early ECRH experiments were done in open field line systems and "line tying" may have played a role in determining stability[10]. In LDX the background plasma is stabilized by an entirely different mechanism: the energy required for the plasma to expand (known as plasma compressibility) in a system characterized by a large magnetic flux expansion.

The observations of stable high beta electron plasmas confined by axisymmetric mirrors are noteworthy because the pressure gradients exceeded the usual criteria for MHD stability. Stability was possible because instabilities driven by fast electrons acquire a real frequency, $\omega \approx m\omega_{dh}$, proportional to the product of the azimuthal mode number, m, and the magnetic drift frequency of the fast electrons. The real frequency induces a stabilizing ion polarization current[13,14] that imposes an instability threshold inversely proportional to the ratio of the line-averaged fast electron and ion densities, $\bar{n}_h/\bar{n}_i$. The high-frequency hot electron interchange (HEI) instability[14] has a mode number, $m \sim 7$, and a real frequency above the ion cyclotron frequency, $\omega \approx m\omega_{dh} > \omega_{ci}$. This mode was observed in bumpy tori, and it destroyed fast electron confinement when $\bar{n}_h/\bar{n}_i \sim 40\%$.[15] The low-frequency HEI instability, first described by Krall[13], was predicted to occur when

$$-\frac{d\ln \bar{n}_{eh}}{d\ln V} > 1 + \frac{m_\perp^2}{24}\frac{\omega_{dh}}{\omega_{ci}}\frac{\bar{n}_i}{\bar{n}_{eh}}. \qquad (1)$$

where $V = \oint d\ell/B$ is the differential volume of a magnetic flux tube and $m_\perp$ is a total perpendicular wavenumber[16] and the over bar represents the flux tube average. Examination of Eq. 1 indicates that the hot electron density gradient is limited most severely at low hot electron energy (since $\omega_{dh} \propto E_{eh}$) and at high hot electron fraction ($\bar{n}_{eh}/\bar{n}_i$). The low-frequency HEI was observed in low beta plasma, $\beta < 1\%$, containing energetic electrons trapped in a supported dipole experiment.[17,18] In the low beta dipole experiment, the HEI appeared with low azimuthal mode number, $m \sim 1$, a broad radial mode structure, and a complex, time-evolving frequency spectrum.[18] Intense bursts of instability induced chaotic radial transport[17], and nonlinear frequency-sweeping was evidence for the inward propagation of "phase-space holes".[19]

In the experiments reported here, the trapped electron beta was also limited by the low-frequency HEI, but when the neutral gas was programmed so as to maintain the deuterium gas pressure between about 1-3 $\times 10^{-6}$ Torr, the fast electron pressure increased by more than a factor of ten and the stable high beta plasma could be maintained for many seconds. The high beta plasma generated a large equilibrium toroidal current, $I_p > 3$ kA, that is analogous to the ring current generated by high beta plasma in the Earth's magnetosphere.[20] Measurements of magnetic field of the plasma current and the location of fast electrons using x-ray imaging constrain models

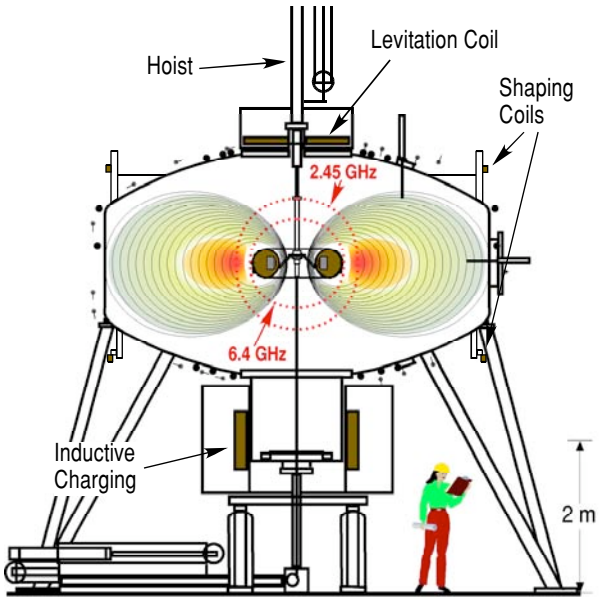

FIG. 1: (Color online) Schematic of LDX experiment showing the dipole magnet suspended within the vacuum vessel. Loops and coils measure the equilibrium plasma current, and probes measure fluctuating potentials. Injected microwave power strongly heats electrons at the cyclotron resonance.

for the anisotropic pressure profile and allow estimates of the plasma stored energy, $W_p > 300$ J, and peak beta, $\beta \approx 20\%$. We also find that the presence of instability creates hysteresis in high-beta plasma behavior. High neutral fueling is required to create a high beta plasma, but, once stabilized, lower neutral fueling is needed to maintain the high beta state.

The remainder of this article is organized into three sections. First, the LDX experiment is described including a general account of the creation of LDX microwave discharges. Next, the equilibrium of the anisotropic fast-electron pressure is parameterized by reconstruction of the plasma diamagnetic current from an array of magnetic sensors. Finally, observations of the hot electron interchange instability that occur at the transitions to and from high and low plasma beta are described together with measurements of the levels of neutral fueling associated with stabilization and instability.

II. DESCRIPTION OF THE LDX EXPERIMENT

As shown in Fig. 1, LDX consists of an internal superconducting coil located within a 5 m dia. vacuum chamber. The coil's dipole moment is $M = 0.34\, I_d$ A·m^2, and experiments have been conducted with I_d ranging from 0.75 and 1.2 MA. A large bore superconducting coil, located below the main chamber, is used to inductively charge the dipole coil. The dipole is lifted for plasma experiments by a vacuum hoist. In this configuration three 1.5 cm dia. support rods intersect the plasma causing

heat and particles to be lost from the plasma. (In future experiments the coil will be magnetically levitated, eliminating losses to the support rods.) Two shaping coils, arranged in a Helmholtz configuration, are located at the outer diameter of the vacuum vessel and may be used to produce a magnetic separatrix. The effect on stability of shaping the outer plasma will be reported elsewhere.

Plasma diagnostics include 26 magnetic sensors to detect the plasma equilibrium current, movable probes to measure electrostatic fluctuations and edge plasma parameters, internal magnetic probes to measure magnetic fluctuations, x-ray and visible light imaging cameras, and a microwave interferometer to measure the line-averaged density across an equatorial path through the plasma. The x-ray camera contains a medical x-ray image intensifier sensitive to energies greater than 45 keV and was previously used during tokamak heating experiments.[21] A standard video camera is used to observe the fast electrons during the afterglow as described in Ref. 12. The magnetic sensors include 19 magnetic field coils and Hall-effect probes and 7 magnetic flux loops attached to the vacuum vessel. Several Langmuir probes can be moved distances up to 0.4 m throughout the edge of the plasma, and two of these probes have high-impedance tips and high-speed amplifiers used to measure the potential fluctuations of the hot electron interchange instability and other lower-frequency perturbations of the plasma.

A. Typical Microwave Discharge

Fig. 2 shows diagnostic signals from a typical LDX high-beta discharge. 5 kW of total ECRH microwave power was applied to the plasma with equal amounts from 2.45 GHz and 6.4 GHz sources. The deuterium pressure was adjusted with four preprogrammed gas puffs. After an initial period lasting 0.25 s, the light emitted from the plasma abruptly increases followed by a more gradual increase in the perturbed magnetic flux near the outer equator. Since this detector senses 0.78 mV·s/kA for a current ring located at 1 m radius, Fig. 2 indicates several kA of equilibrium plasma current. Measurements using a microwave interferometer show the light emission is roughly proportional to the plasma line-density. By viewing the dipole magnet from several directions, we know x-rays result from plasma bremsstrahlung and from fast electrons driven inward to the dipole magnet. When the ECRH power is switched off, the plasma equilibrium current slowly decays proportional to the collisional loss rate of the trapped electrons.

B. Three Regimes of the LDX Plasma

The time evolution of plasma discharges created in LDX show the plasma to exist within one of three plasma regimes: the "low density" regime ($0 < t < 0.25$ s), the "high beta" regime ($0.25 < t < 4$ s), and the "afterglow " ($t > 4$ s) that occurs after the ECRH power is switched off. These three characteristic regimes are indicated in Fig. 2 with the letters, "LD", "HB", and "AG".

In the low density regime, the plasma is characterized by relatively small diamagnetism (~ 0.1 mV·s) and line-density ($\sim 2.3 \times 10^{16}$ m^{-3}). Fig. 2 shows evidence of rapid radial transport. A significant x-ray signal is observed on a NaI detector with a radial view that includes the floating coil, which indicates inward-moving hot electrons striking the surface of the dipole coil. Negatively biased Langmuir probes at the outer edge of the plasma measure intense bursts of outward-directed energetic electrons. High-speed recordings of the electrostatic potential fluctuations (described in Sec. 4) show frequencies that resonate with the magnetic drifts of electrons with energies ranging from 20-60 keV. As observed previously in a supported dipole experiment,[17–19] the HEI instability appears as quasi-periodic bursts with frequencies that are $\approx 0.3\omega_{dh}$ and sweep to higher frequencies, $\omega \sim 1.8\omega_{dh}$, during the nonlinear saturation of the instability. Visible light images of "low density" discharges show the light emission is localized to the equatorial plane indicating a strong interaction between the plasma and the limiter on the outside of the floating coil, and the formation of a "disk" of deeply-trapped hot electrons. When the instability bursts become intense, the video images show inward transport of energetic plasma causing removal of dust and material from the dipole coil and its supports as indicated in Fig.2b. X-ray images show a strong x-ray emission at the outer floating coil limiter further indicating an inward transport of hot electrons. We conclude from these observations that the low density regime is associated with a quasi-continuous presence of hot electron interchange instability that causes rapid radial transport of energetic electrons.

The high-beta regime occurs after an abrupt transition that occurs when the neutral gas pressure exceeds a critical level that ranges from 2.5-3.5$\times 10^{-6}$ Torr. The level of neutral gas pressure required for the transition increases with the level of microwave heating power and varies when the outer shape of the plasma is modified. Typically the transition occurs rapidly, within 2 ms, and coincides with the ionization of the background neutrals and a rapid buildup of plasma density to a value 7-10 times larger than during the low-density regime. A 10-20 fold buildup of plasma diamagnetism occurs over a much longer interval, ~ 0.5 s. Initially, as the density rises, the detected x-ray intensity decreases by an order of magnitude consistent with the elimination of inward hot electron flux to the floating coil. The sign of the current collected by the negatively-biased edge probes reverses, so that positive ion saturation current is collected, indicating a sharp decrease in radial transport of fast electrons. As will be described in Sec. 4, high-speed floating potential probe measurements show the HEI instability is stable after the transition to the high-beta regime.

Although the high-beta regime is grossly stable when

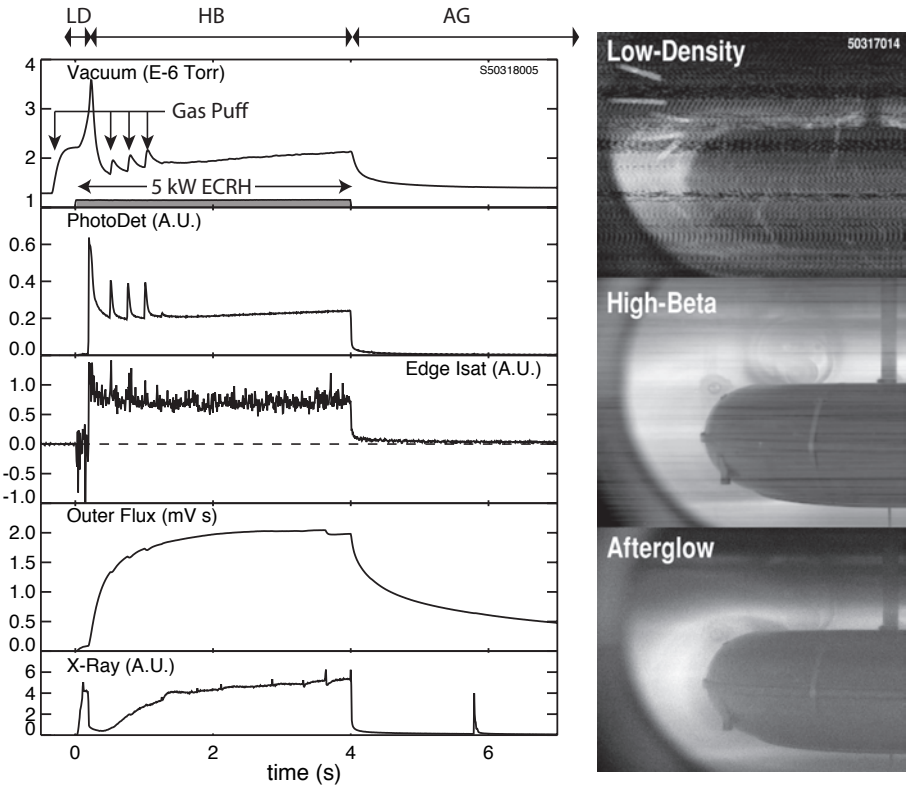

FIG. 2: Example high beta plasma discharge created with 5 kW ECRH power and four gas puffs. (Left) Measurements show (i) the deuterium gas pressure within the chamber, (ii) the visible light from the plasma, (iii) the measured current from a negatively-biased Langmuir probe at the plasma edge, (iv) the magnetic flux near the outer equator, and (v) the x-ray intensity. (Right) Visible light frames from the low density, high beta and afterglow plasmas.

compared to the low-density regime, infrequent and relatively short bursts of HEI fluctuations occur at a rate determined by the levels of neutral fueling and microwave power. In Fig. 2, these small bursts are seen on the x-ray intensity signal and are sometimes accompanied by small drops in stored energy. This indicates that the high-beta plasma remains close to marginal stability. Video images show "high-beta" plasmas do not cause particles to be removed from the dipole coil surfaces, but instead shows an increased glow of the three coil support rods indicating the power deposition to the support rods increases during the high-beta regime. During the high beta regime, magnetic and electrostatic fluctuations appear that are easily distinguished from the HEI instability since the observed frequencies are below 5 kHz and are not associated with strong radial transport.

When the microwave power is switched off, the plasma evolves to the regime called the "afterglow". The plasma density decays within 10-15 ms, while the energetic trapped electron population decays much more slowly (1-20 s) consistent with the pitch angle scattering rate of hot electrons. The slow decay of the diamagnetism indicates that the bulk of the stored energy is contained in the hot electron population while the fast decay of plasma density indicates that a significant fraction of the injected microwave power is required to maintain the density of the cooler plasma. During the afterglow, video images of the plasma show a crescent shaped light emission indicating a broadening of the hot electron pitch angle distribution as compared to the low density and high-beta discharge regimes. The behavior of the afterglow plasma also depends upon the level neutral pressure. If the neutral pressure during the afterglow decreases, very intense bursts of HEI instability appear that cause can lead to the complete destruction of fast electron confinement and loss of trapped energy.

III. CHARACTERIZING THE HIGH BETA PLASMA

The high beta hot-electron plasma component forms a ring that is localized close to the field minimum (*i.e.* on the outer midplane) at the ECH resonance location. The diamagnetic currents that determine plasma equilibrium also peak on the outer midplane and change sign on either side of the pressure peak. Estimates of the plasma pressure are made by computing the least-squares best-fit of a model to the magnetic diagnostics. We use an anisotropic pressure profile, with $P_\perp > P_{||}$, that is similar to that used to study plasma equilibrium and stability in the magnetic field of a point dipole[24,25] and given by

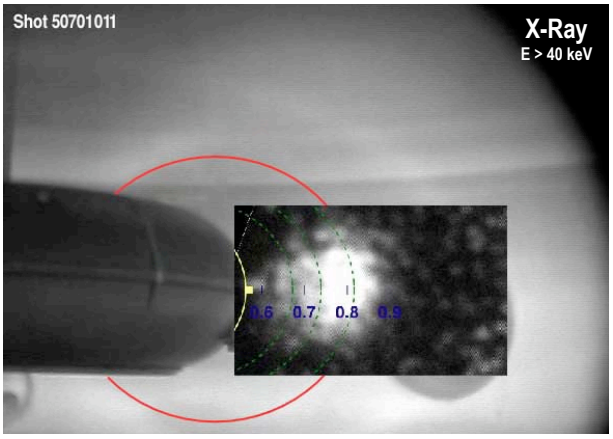

FIG. 3: (Color online) Superposition of the measured x-ray intensity and the visible light for single-frequency, 2.45 GHz, ECRH. The x-ray image shows localization of fast-electrons.

$P_\perp(\psi, B) = \hat{P}(\psi)(B_0(\psi)/B)^{2p}$ where $\mathbf{B} = \nabla\phi \times \nabla\psi/2\pi$ and $B_0(\psi)$ is the minimum field strength on a field-line. With this model, the ratio of perpendicular to parallel pressure is a constant, $P_\perp/P_{||} = 1 + 2p$. To fit this model to the magnetic measurements, the plasma current, $J_\phi(r, z)$ is related to the pressure through the self-consistent equilibrium, $\psi(r, z)$. However, since the dipole moment of J_ϕ is less than 2% of the coil's magnetic moment, the difference between J_ϕ computed using the vacuum dipole field and the self-consistent field is undetectable for the beta achieved to date. Using the dipole's vacuum field, the plasma ring current density can be computed from any given function of $\hat{P}$ and parameter p using $J_\phi = -2\pi r\,[D_\psi P_\perp + 2pP_\perp D_\psi \ln B/(1+2p)]$, where $D_\psi \equiv |\nabla\psi|^{-2}\nabla\psi\cdot\nabla$. The detected signal from a magnetic sensor is computed by combining contributions from J_ϕ throughout the plasma with the decrease of I_d required to maintain constant the flux linked by the superconducting dipole. For the reconstructions reported here, $\hat{P} = \Delta(\psi) \times P_0(\psi/\psi_0)^{4g}$, where $\Delta(\psi) = [(\psi - \psi_d)/(\psi_0 - \psi_d)]^\alpha$ is chosen to vanish at the surface of the dipole, ψ_d, and to equal unity at the location of the pressure peak, ψ_0. Far from the coil's surface, $|\psi| \ll |\psi_d|$, the equatorial pressure is $P_\perp(r) \approx P_0(R_{peak}/r)^{4g}$. This form resembles the MHD condition for marginal stability, expressed as $\delta(PV^\gamma) = 0$ with $\gamma = 5/3$, that is equal to $P \sim r^{-4\gamma}$ in a dipole.[3–6,25]

The radial location of the fast electron population is viewed by an x-ray camera during times when the ECRH is on (Fig. 3) and by a visible camera that detects the ionization glow of the trapped electrons after the microwave heating pulse ends. For single-frequency ECRH, the cameras indicate the pressure peak is localized on the equatorial midplane of the fieldlines having the fundamental cyclotron resonance at the minimum B. This is expected for ECRH since electrons mirror-trapped at resonance are continuously heated by the injected microwaves.[22,23] When both 2.45 GHz and 6.4 GHz sources are on, the

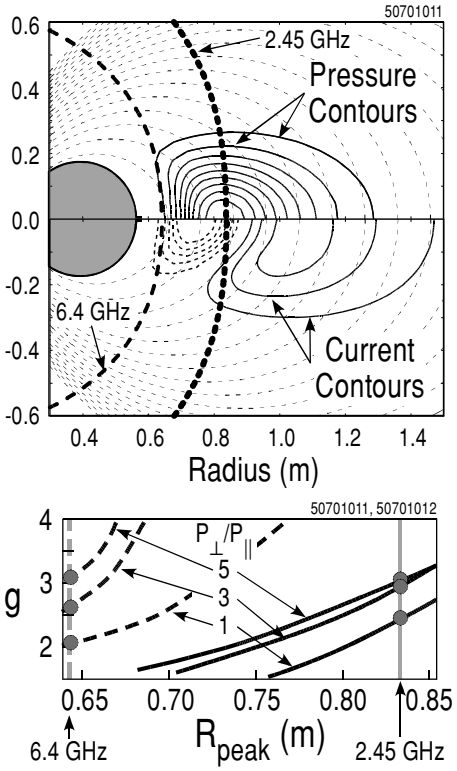

FIG. 4: Magnetic reconstruction of plasma pressure and current profiles for ECRH with 2.45 GHz microwaves. (Top) Pressure and current contours for the "best-fit" anisotropic profile, $p_\perp/p_{||} = 5$. (Bottom) Profile factor, g, that best fits magnetic measurements as a function of the radius of the pressure peak and plasma anisotropy.

x-ray image shows the fast electrons localized at the equator but spanning both resonances in the radial direction.

Fig. 4 illustrates the model pressure and current profiles that are the least-squares best fit to the magnetic measurements of high beta plasma produced with single-frequency ECRH. We find equally good fits occur either with steep profiles centered at large radii or with broad profiles centered at smaller radii. This results because J_ϕ is primarily determined from the pressure gradient and the magnetic sensors are most sensitive to the plasma's dipole moment. When only 2.45 GHz heating is applied (solid lines in Fig. 4b), very good fits result with $1.7 < g < 3.1$ when $0.68 < R_{peak} < 0.85$. Because we observe the fast-electron population to peak at the ECRH resonance, $R_{peak} = 0.83$ m, we conclude $g = 2.0,\ 2.8,\ 3.1$ for $p = 0,\ 1,\ 2$, respectively. When only 6.4 GHz microwaves are applied, $R_{peak} = 0.64$ m, and $g = 2.0,\ 2.8,\ 3.5$ for $p = 0,\ 1,\ 2$. Because of the dipole support rods, $p > 0$. From this, previous experiments[11,12], and the measured height of the x-ray images, we believe the pressure is well approximated by $P_\perp/P_{||} \sim 5$. Fig. 4a show the model $P_\perp$ and J_ϕ profiles that best fit measurements.

Plasma with the highest values of I_p and β are created

TABLE I: Measured and reconstructed parameters characterizing high-beta LDX plasma produced with ECRH.

Dipole current (MA)	0.93
2.45 GHz microwave power (kW)	2.5
6.4 GHz microwave power (kW)	2.5
Plasma stored energy (J)	330
Plasma volume (m^3)	29
Total plasma current (kA)	3.5
Change of dipole current (kA)	−0.80
Location of pressure peak, R_{peak} (m)	0.72
Adiabatic profile parameter, g	2.8
Anisotropy, $P_\perp/P_{||}$	5
Current centroid (m)	1.2
Plasma dipole moment (kA·m^2)	4.8
Best-fit peak beta, β_{max} (%)	21
Volume-averaged beta, $\langle\beta\rangle$ (%)	1.7
Peak perpendicular pressure (Pa)	750
Fast electron energy, E_h (keV)	100-250
Fast electron density, n_h ($\times 10^{16}$ m^{-3})	2-4
Line density ($\times 10^{19}$ m^{-2})	1.8
Edge electron temperature (eV)	10
Edge density ($\times 10^{16}$ m^{-3})	0.6-1.0

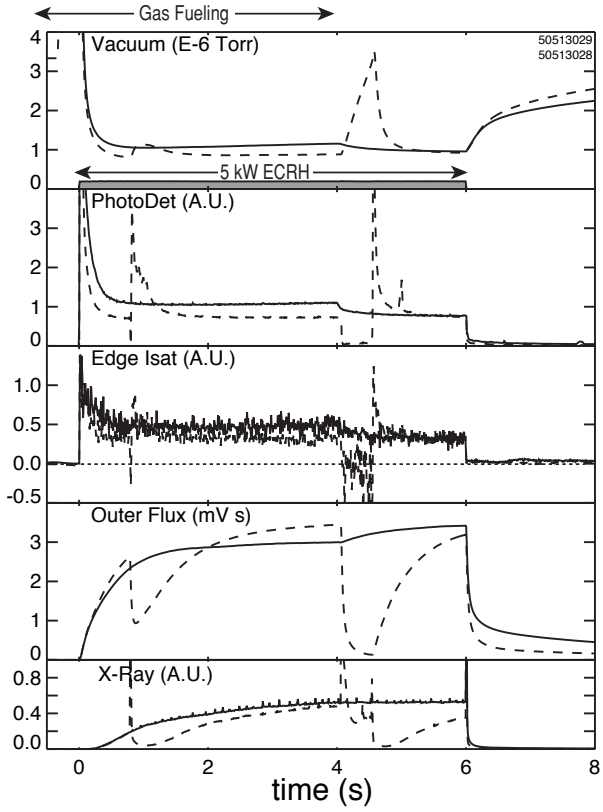

FIG. 5: Consecutive discharges, Nos. 50513028 (dotted line) and 50513029 (solid line), in which gas feed is increased by 15%. From top to bottom, the measurements are (a) vacuum pressure, (b) visible light intensity proportional to plasma line density, (c) edge ion saturation current, (d) plasma diamagnetic flux, and (e) x-rays intensity.

with both 2.45 GHz and 6.4 GHz heating. The sum of the mean-square deviations between the best-fit model profile and the magnetic measurements doubles as compared with single-frequency heating, and this may be related to the presence of two pressure peaks, one at each resonance. If R_{peak} is assumed to be midway between the resonances and $p = 2$, then 5 kW of heating creates a plasma (discharge No. 50513029) with $I_p = 3.5$ kA, $\Delta I_f = -0.8$ kA, $W_p = 330$ J, $g = 2.8$, peak perpendicular pressure of 750 Pa, and maximum local beta of $\beta = (2\beta_\perp + \beta_{||})/3 = 21\%$. If R_{peak} moves outward closer to the 2.45 GHz resonance by 5 cm, $\beta = 23\%$; moving inward by 4 cm towards the 6.4 GHz resonance, the best-fit results in $\beta = 18\%$.

Table 1 shows the equilibrium parameters for high-beta discharge No. 50513029 produced with a total injected heating power of 5 kW of equal amounts from the 2.45 and 6.4 GHz microwave sources.

IV. MAINTAINING STABILITY WITH CONTROLLED GAS FUELING

The transition to and from the high beta regime warrants discussion. In Fig. 5, two consecutive discharges are shown in which the gas fueling is increased by 15% for the second shot, 50513029, as compared with the previous one. When the neutral fueling was lower, in discharge 50513028, the high-beta plasma does not remain stable as indicated by the rapid reductions of the diamagnetic flux observed at $t = 0.8$ s and at $t = 4$ s. The first event causes approximately half of the trapped electrons to be loss, and the second event results in nearly complete loss of fast electron confinement. The unstable losses of trapped energetic electrons occur when the neutral gas pressure falls below a critical value, $\sim 1 \times 10^{-6}$ Torr. The loss events are accompanied by negative current to the edge probe, by bright x-ray flashes indicating inward fast electron transport, and by rapid decrease in plasma density. Fig. 6b shows details for the loss event at near 0.8 s. When the neutral pressure in the chamber decreases sufficiently, an intense burst of HEI instability initiates at $t = 0.791$ s. The first millisecond of the growing instability appears with broad spectral content ($0.2 < \omega/2\pi < 6$ MHz) and resonates with fast electrons having a wide range of energies that extend beyond 200 keV. During this interval, a large flux of energetic electrons is detected with a negatively-biased edge probe. At $t = 0.792$ s, the amplitude of the HEI instability saturates and coherent nonlinear frequency sweeping occurs, with associated bright light and x-ray emission indicating fast electron impact with the dipole. The frequency spectrum, induced fast electron transport, and azimuthal

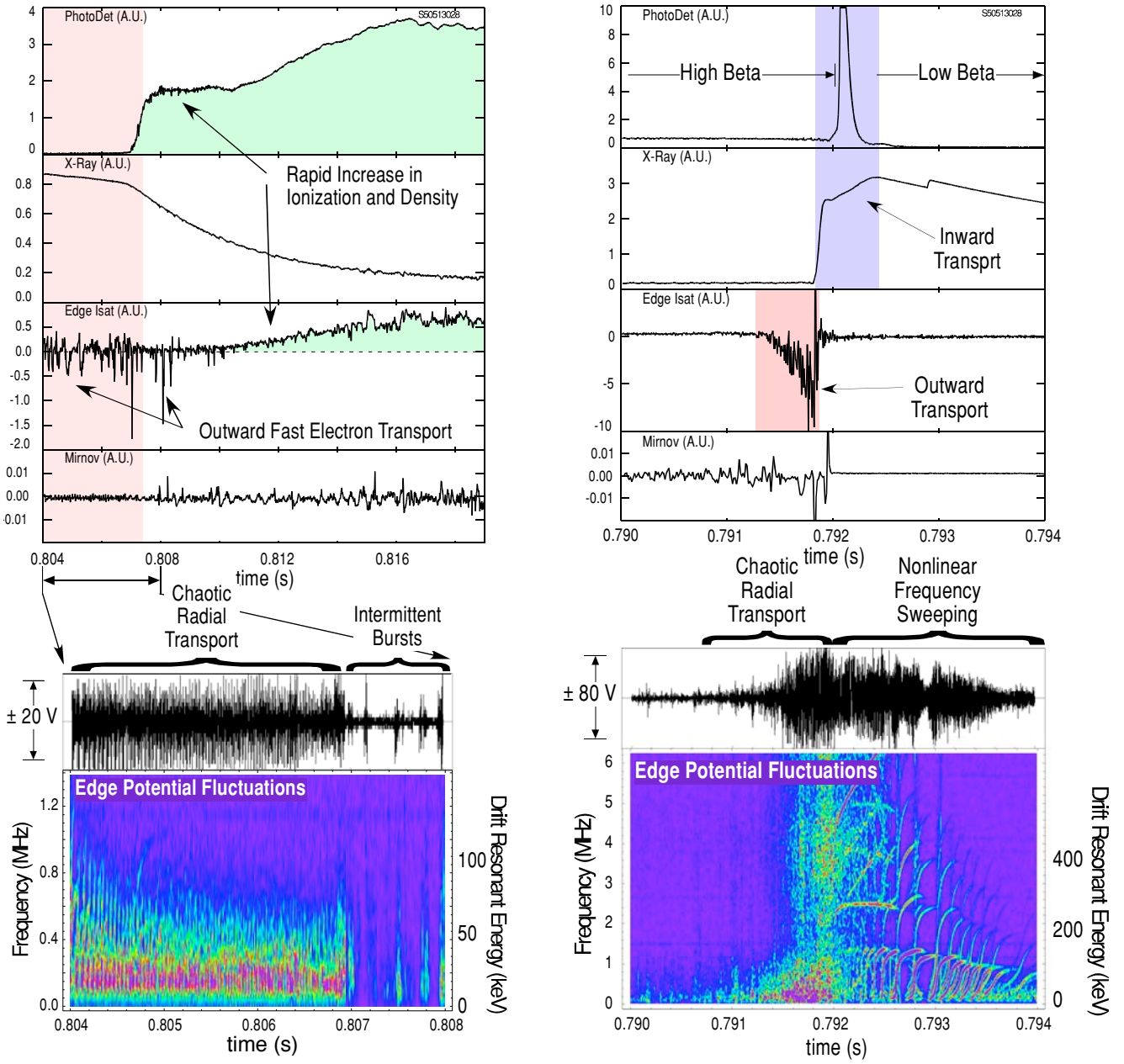

FIG. 6: (Color) A transition to the high beta regime (left) and an unstable transition from high-beta to low-beta (right) seen in discharge 50513028. Each transition is illustrated with measurements of (i) visible light, (ii) target x-ray signal, (iii) edge ion saturation current, (iv) Mirnov magnetic fluctuation signal, (v) edge potential fluctuation signal, and (vi) frequency-time plot for potential fluctuations.

mode structure of these fluctuations resemble previous observations of the HEI instability in a dipole[17,18].

The intense HEI instability burst also leads to a rapid loss of plasma density, and the discharge enters the low-density regime with quasi-continuous HEI fluctuations near $\omega/2\pi \sim 0.2$ MHz. As the neutral pressure in the plasma rises and reaches $\sim 1.4\times10^{-6}$ Torr at $t = 0.807$ s, the HEI becomes stable (Fig. 6a), followed by a rapid rise in density, a drop in x-ray intensity, and a termination of the fast-electron current at the edge probe. The difference between the neutral pressure required for these two transitions constitutes a hysteresis that results from the cross field radial transport caused by the HEI instability.

Fig. 7 shows a discharge with low levels of neutral gas fueling where five transitions to and from the high-beta regime were recorded. The radial transport induced by the instability creates hysteresis in the neutral gas fueling required to maintain sufficient density to stabilize high

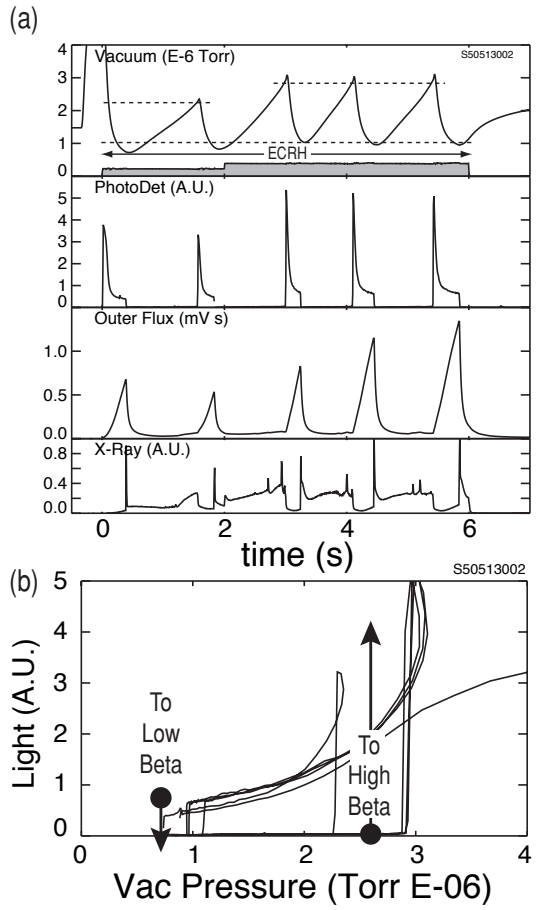

FIG. 7: (a) Discharge 50513002 in which a series of transitions between high beta and low-density operation caused by HEI instability. Vacuum pressure, visible light, diamagnetism and x-ray signals are shown. In (b), the evolution of three discharges are shown: one, with higher fueling, is always stable; two, with less fueling, have transitions to stability (at 2-3 $\times 10^{-6}$ Torr) and unstable HEI transitions to low beta (at 1×10^{-6} Torr).

beta plasma. Once the pressure threshold is exceeded, the plasma density and visible light abruptly increase and the HEI immediately stabilizes. The hysteresis caused by the relationship between plasma density and fast electron stability is shown in Fig. 7b. As shown in Fig. 7, this pressure threshold depends upon the ECRH power level. At 2 kW, the HEI is stabilized and the transition to high beta occurs at a pressure just above 2×10^{-6} Torr. At 4 kW and 5 kW, the transition pressures are 2.8 and 3.2×10^{-6} Torr. Once the plasma enters the higher density, high beta state, the high-beta electrons remain grossly stable so long as the neutral pressure remains above 1×10^{-6} Torr. When the pressure drops below the threshold the fast electron confinement is destroyed and the plasma density and beta essentially disappear within a few msec. At high beta, the HEI fluctuations can resonate with the drift motion of electrons with high energies $E_h > 100$ keV; whereas, at low beta, the fluctuations resonate with lower-energy electrons, $E_h < 60$ keV.

The transition to the stable high beta regime and the subsequent plasma buildup may be understood qualitatively from a simple point model:

$$\frac{d\bar{n}_{eb}}{dt} = \bar{n}_0(\bar{n}_{eb}\langle\sigma_{ic}v\rangle + \bar{n}_{eh}\langle\sigma_{ih}v\rangle) - \bar{n}_{eb}/\tau_{ECRH} - \bar{n}_{eb}/\tau_X - \frac{\bar{n}_{eb}^2}{\langle n\tau_{eb}\rangle} \quad (2)$$

$$\frac{d\bar{n}_{eh}}{dt} = \bar{n}_{eb}/\tau_{ECRH} - \bar{n}_{eh}/\tau_X - \frac{\bar{n}_{eh}(\bar{n}_0 + \bar{n}_{eb} + \bar{n}_{eh})}{\langle n\tau_{eh}\rangle} \quad (3)$$

with $\bar{n}_{eb}$ the flux-tube averaged "bulk", or non-energetic, electron density, $\bar{n}_0$ the neutral density, τ_{ECRH} and τ_X respectively the characteristic time for cross field transport and ECRH heating of bulk electrons to the high energy of the trapped fast electrons. The ionization source, proportional to $\bar{n}_0$ will compete with ECRH-induced diffusion which promotes electrons up to high energies as well as with cross field transport and loses along the field to supports. For insufficient neutral density, the ECRH promote a large fraction of electrons to high energy and $\bar{n}_{eh}/\bar{n}_{eb} \approx \tau_X/\tau_{ECRH} \sim 1$. The plasma density is determined by the absorbed microwave power and plasma volume, $P_{ECRH}/V \propto E_h\bar{n}_{eb}/\tau_{ECRH} \sim E_h\bar{n}_{eh}/\tau_X$. This results in a plasma with a large fast electron fraction, $\bar{n}_{eh}/\bar{n}_i \sim 0.5$, that is strongly unstable to HEI instability. (See Eq. 1.) For sufficient neutral density, the source of bulk electrons exceeds the loss rate, resulting in a rapid buildup of plasma density and stabilization of the HEI instability. In this case, $1/\tau_X \to 0$, and $\bar{n}_{eb}$ is determined by a balance between the absorbed microwave power, P_{ECRH} consistent with accessibility, and the power required to ionize and to supply the plasma losses to the dipole supports. As a consequence of the larger plasma density, the fast electron production rate, $\bar{n}_{eb}/\tau_{ECRH}$, is reduced; however, a fraction of the heating power is directly absorbed by the fast electrons, increasing E_h by at least a factor of four from the low-density regime. Thus, the increased plasma density resulting from higher neutral pressure produces high-beta fast electrons that have at least twice the density and four times the energy as the low-density regime. Stability is possible since $\bar{n}_{eh}/\bar{n}_i \sim 0.1$, much lower than found in the low-density regime. Additionally, the very simple point model represented by Eqs. 2 and 3 indicates: (i) a critical neutral density is required to permit plasma density build up, (ii) higher levels of ECRH power require higher values of neutral pressure to permit buildup, (iii) once there exists sufficient fueling for density buildup any further increase in neutral density only adds to the collisional scattering loss of the trapped electrons to the dipole supports, (iv) once the fast electron fraction is reduced to the level that stabilizes the HEI mode, cross field transport will decrease leading to a "hysteresis" in plasma behavior as gas fueling changes. An implication of this model is that

when the dipole coil is levitated (in future experiments) the scattering loss to the supports will be eliminated, and there should be a reduction in the neutral pressure required for density buildup and a significant improvement in the energy confinement of microwave-heated plasma.

V. CONCLUSION

A stable high-beta plasma containing fast energetic electrons has been created and sustained in a laboratory dipole experiment using 5 kW of ECRH power and controlled neutral gas fueling. X-ray images show the high beta trapped electrons to be localized at the fundamental cyclotron resonance. The plasma current calculated from model anisotropic pressure profiles are fit to magnetic measurements and indicate the peak local beta reaches 20%. If the neutral gas fueling is insufficient, HEI instabilities either prevent the buildup of fast-electron beta or rapidly destroy fast-electron confinement. In the stable high beta mode of operation, losses of both the fast electron (high beta) component and the background plasma are dominated by scattering losses to the dipole supports.

In upcoming experiments, the superconducting dipole will be magnetically levitated, and we anticipate plasma confinement will significantly improve since all loss processes will involve cross-field radial transport. With improved plasma confinement, less neutral pressure will be needed to insure the plasma density is sufficiently high for fast-electron drift stability. The plasma beta would rise further, and the plasma pressure profile would become more isotropic.

Acknowledgments

We gratefully acknowledge the technical expertise of V. Fishman, R. Lations, J. Minervini, D. Strahan, A. Zhukovsky, and S. Zweben. This work was supported by US DOE Grants DE-FG02-98ER54458 and DE-FG02-98ER54459.

* Electronic address: garnier@mit.edu

[1] J. Kesner, L. Bromberg, D.T. Garnier, M.E. Mauel, in *Fusion Energy 1998* (IAEA, Vienna, 1999) **3**, 1165. (1999)
[2] A. Hasegawa, Comments Plasma Phys. Controlled Fusion, **1**, 147 (1987).
[3] M.N. Rosenbluth and C.L. Longmire, Ann. Phys. **1**, 120 (1957).
[4] I.B. Bernstein, E. Frieman, M. Kruskal, R. Kulsrud, Proc. R. Soc. Lond. A **244**, 17 (1958).
[5] T. Gold, J. Geophys. Res., **64**, 123 (1959).
[6] D.T. Garnier, J. Kesner, M.E. Mauel, Phys. Plasmas **6**, 3431 (1999).
[7] J. Kesner, D.T. Garnier, A. Hansen, M. Mauel, L. Bromberg, Nucl. Fusion **44**, 193 (2004).
[8] R. A. Dandl, A. C. England, W. B. Ard, H. O. Eason, M. C. Becker, and G. M. Hass, Nuc. Fusion, **4**, 344 (1964).
[9] R. A. Dandl, F. W. Baity Jr., K. H. Carpenter, J. A. Cobble, H. O. Eason, *et al.*, Nuc. Fusion, Suppl., **2**, 355 (1979).
[10] A.J. Lichtenberg and H. Meuth, Phys. Fluids, **29**, 3511 (1986).
[11] B. H. Quon, R. A. Dandl, W. DiVergilo, G. E. Guest, L. L. Lao, *et al.*, Phys. Fluids, **28**, 1503 (1985).
[12] X. Chen, B. G. Lane, D. L. Smatlak, R. S. Post, and S. A. Hokin, Phys. Fluids B, **1**, 615 (1989).
[13] N. Krall, Phys. Fluids, **9**, 820 (1966).
[14] H.L. Berk, Phys. Fluids, **19**, 1275 (1976).
[15] S. Hiroe, J. B. Wilgen, F. W. Baity, L. A. Berry, *et al.*, Phys. Fluids, **27**, 1019 (1984).
[16] M.E. Mauel, Journal de Physique, IV **7**, 307 (1997).
[17] H. P. Warren, M. E. Mauel, Phys. Rev. Lett., **74** (1995) 1351; and H. P. Warren and M. E. Mauel, Phys. Plasmas **2**, 4185 (1995) .
[18] B. Levitt, D. Mastovsky, and M.E. Mauel, Phys. Plasmas **9**, 2507 (2002).
[19] D. Maslovsky, B. Levitt, and M. E. Mauel, Phys. Rev. Lett., **90**, 185001 (2003).
[20] I. A. Daglis, R. M. Thorne, W. Baumjohann, and S. Orsini, Rev. Geophys., **37**, 4 (1997).
[21] S. von Goeler, S. Jones, R. Kaita, S. Bernabei, *et al.*, Rev. Sci. Instr., **65**, 1621 (1994).
[22] D. Batchelor, Nuc. Fusion **21**, 1615 (1981).
[23] M. E. Mauel, Phys. Fluids, **27**, 2899 (1984).
[24] S.I. Krasheninnikov and P.J. Catto, Phys. Plasmas, **7**, 626 (2000).
[25] A.N. Simakov, R. J. Hastie, and P.J. Catto, Phys. Plasmas, **7**, 3909 (2000).